

Article

Theoretical and Experimental Nucleation and Growth of Precipitates in a Medium Carbon–Vanadium Steel

Sebastián F. Medina ^{1,*}, Inigo Ruiz-Bustanza ¹, José Robla ¹ and Jessica Calvo ²

¹ National Centre for Metallurgical Research (CENIM-CSIC), Av. Gregorio del Amo 8, 28040 Madrid, Spain; irbustanza@cenim.csic.es (I.R.-B.); jrobla@cenim.csic.es (J.R.)

² Technical University of Catalonia (ETSEIB—UPC), Av. Diagonal 647, 08028 Barcelona, Spain; jessica.calvo@upc.edu

* Correspondence: smedina@cenim.csic.es; Tel.: +34-91-5538-900

Academic Editor: Hugo F. Lopez

Received: 10 November 2016; Accepted: 30 January 2017; Published: 7 February 2017

Abstract: Using the general theory of nucleation, the nucleation period, critical radius, and growth of particles were determined for a medium carbon V-steel. Several parameters were calculated, which have allowed the plotting of nucleation critical time vs. temperature and precipitate critical radius vs. temperature. Meanwhile, an experimental study was performed and it was found that the growth of precipitates during precipitation obeys a quadratic growth equation and not a cubic coalescence equation. The experimentally determined growth rate coincides with the theoretically predicted growth rate.

Keywords: microalloyed steel; nucleation time; nucleus radius; precipitate growing

1. Introduction

During the hot deformation of microalloyed steels an interaction takes place between the static recrystallization and precipitation of nanometric particles, which grow until reaching a certain size. The complexity of this phenomenon has been studied by many researchers and is influenced by all the external (temperature, strain, strain rate) and internal variables (chemical composition, austenite grain size) that participate in the microstructural evolution of hot strained austenite [1–8].

First of all, the precipitates nucleate and then increase in size by means of growth and coarsening or coalescence [9]. During coarsening, the largest particles grow at the expense of the smallest, and according to some authors this takes place due to the effect of accelerated diffusion of the solute along the dislocations, i.e., when the precipitation is strain-induced [10].

The present work basically addresses the precipitation in a vanadium microalloyed steel, distinguishing the growth and coarsening phases and determining which of these phenomena is really the most important for the increase in precipitate size. Calculations have been performed taking into account the general theory of nucleation [11,12].

Comparison of the calculated and experimentally obtained results helps to understand the precipitation phenomenon in its theoretical and experimental aspects, respectively.

2. Materials and Methods

The steel was manufactured by the Electroslag Remelting Process and its composition is shown in Table 1, which includes an indication of the $\gamma \rightarrow \alpha$ transformation start temperature during cooling (A_{F3}), determined by dilatometry at a cooling rate of 0.2 K/s, which is the minimum temperature at which the different parameters related with austenite phase precipitation will be calculated.

Table 1. Chemical composition (mass %) and transformation critical temperature (A_{r3} , 0.2 K/s).

C	Si	Mn	V	N	Al	A_{r3} , °C
0.33	0.22	1.24	0.076	0.0146	0.011	716

The specimens for torsion tests had a gauge length of 50 mm and a diameter of 6 mm. The austenitization temperature was 1200 °C for 10 min, and these conditions were sufficient to dissolve vanadium carbonitrides. The temperature was then rapidly lowered to the testing temperature of 900 °C, where it was held for a few seconds to prevent precipitation taking place before the strain was applied. After deformation, the samples were held for times of 50 s, 250 s, and 800 s, respectively, and finally quenched by water stream. The parameters of torsion, torque, and number of revolutions, and the equivalent parameters, stress and strain, were related according to the Von Mises criterion. Accordingly, the applied strain was 0.35, and the strain rate was 3.63 s⁻¹.

A transmission electron microscopy (TEM) (CM20 TEM/STEM 200KV, Philips, Eindhoven, The Netherlands) study was performed and the carbon extraction replica technique was used. The distribution of precipitate sizes was always determined on a population of close to 200 precipitates. This technique is widely used, but there are other competitive techniques such as quantitative X-ray diffraction (QXRD) [13].

3. Results and Discussion

3.1. Theoretical Model and Calculation of Parameters

The Gibbs energy for the formation of a spherical nucleus of carbonitride from the element in solution (V) is classically expressed as the sum of chemical free energy, interfacial free energy, and dislocation core energy, resulting in the following expression [14–16]:

$$\Delta G(J) = \frac{16\pi\gamma^3}{3\Delta G_v^2} + 0.8\mu b^2 \frac{\gamma}{\Delta G_v} \quad (1)$$

where γ is the surface energy of the precipitate (0.5 Jm⁻²), ΔG_v is the driving force for nucleation of precipitates, b is the Burgers vector of austenite, and μ is the shear modulus. For austenite, $b = 2.59 \times 10^{-10}$ m and $\gamma = 4.5 \times 10^4$ MPa [9].

The equilibrium between the austenite matrix and the carbonitride VC_yN_{1-y} is described by the mass action law [15]:

$$\Delta G_v \left(J \cdot m^{-3} \right) = -\frac{R_g T}{V_m} \left[\ln \left(\frac{X_V^{ss}}{X_V^e} \right) + y \ln \left(\frac{X_C^{ss}}{X_C^e} \right) + (1-y) \ln \left(\frac{X_N^{ss}}{X_N^e} \right) \right] \quad (2)$$

where X_i^{ss} are the molar fractions in the solid solution of V, C, and N, respectively, X_i^e are the equilibrium fractions at the deformation temperature, V_m is the molar volume of precipitate species, R_g is the universal gas constant (8.3145 J·mol⁻¹·K⁻¹), and T is the deformation absolute temperature.

The carbonitride is considered as an ideal mix of VC and VN, and the values of parameters (y ; X_V^e ; X_C^e ; X_N^e) are determined using FactSage (Developed jointly between Thermfact/CRCT (Montreal, QC, Canada) and GTT-Technologies (Aachen, Germany)) [17,18]. The value of “ y ” in Equation (4) is the precipitated VC/VCN ratio, and “ $1 - y$ ” is the VN/VCN ratio. On the other hand, $N_0 = 0.5 \Delta\rho^{1.5}$ is the number of nodes in the dislocation network, $\Delta\rho = (\Delta\sigma/0.2\mu b)^2$ is the variation in the density of dislocations associated with the recrystallization front movement in the deformed zone at the start of precipitation [9], and $\Delta\sigma$ is the difference between the flow stress and yield stress at the deformation temperature.

The atomic impingement rate is given as [10]

$$\beta' \left(\text{s}^{-1} \right) = \frac{4\pi R_c^2 D_V C_V}{a^4} \quad (3)$$

where D_V is the bulk diffusivity of solute atoms (V) in the austenite, a is the lattice parameter of the precipitate, and C_V is the initial concentration of vanadium in mol fraction. Here, the bulk diffusion coefficient (D_V) is replaced by an effective diffusion coefficient, D_{eff} , expressed as a weighted mean of the bulk diffusion (D_V) and pipe diffusion (D_p) coefficients, and used in the description of the precipitate evolution [10,19]:

$$D_{\text{eff}} = D_p \pi R_{\text{core}}^2 \rho + D_V \left(1 - \pi R_{\text{core}}^2 \rho \right) \quad (4)$$

where R_{core} is the radius of the dislocation core, taken to be equal to the Burgers vector, b .

The Zeldovich factor Z takes into account that the nucleus is destabilised by thermal excitation compared to the inactivated state and is given as [20]

$$Z = \frac{V_{\text{at}}^{\text{p}}}{2\pi R_c^2} \sqrt{\frac{\gamma}{kT}} \quad (5)$$

The flow stress increment ($\Delta\sigma$) has been calculated using the model reported by Medina and Hernández [21], which facilitates the calculation of flow stress. The dislocation density has been calculated at the nose temperature of the P_s curve corresponding to a strain of 0.35. When the austenite is not deformed the dislocation density is approximately 10^{12} m^{-2} [22]. The dislocation density corresponding to the curve nose will be given by $10^{12} + \Delta\rho$.

The incubation time (τ) is given as follows [23,24]:

$$\tau = \frac{1}{2\beta'Z^2} \quad (6)$$

The critical radius for nucleation is determined from the driving force and is given as [10]

$$R_c = -\frac{2\gamma}{\Delta G_v} \quad (7)$$

It is obvious that the nuclei that can grow have to be bigger than the critical nucleus, and in accordance with Dutta et al. [9] and Perez et al. [25] this value will be multiplied by 1.05. It must be noted that the factor 1.05 has little consequence on the overall precipitation kinetics.

The integration of Zener's equation for the growth rate will give the radius of the precipitates as a function of time [15]:

$$R^2 = R_0^2 + 2D_{\text{eff}} \frac{X_V^{\text{SS}} - X_V^{\text{i}}}{\frac{V_{\text{Fe}}}{V_{\text{p}}} - X_V^{\text{i}}} \Delta t \quad (8)$$

where V_{Fe} is the molar volume of austenite, V_{p} is the molar volume of precipitate, R is the precipitate radius after a certain time Δt , and R_0 is the average critical radius of the precipitates that have nucleated during the incubation period, coinciding with $1.05R_0$.

The FactSage software tool for the calculation of phase equilibria and thermodynamic properties makes it possible to predict the formation of simple precipitates (nitrides and carbides) and more complex precipitates (carbonitrides), and the results can be expressed as a weight fraction versus temperature [26]. The FSstel database containing data for solutions and compounds [26] was used. The calculations were carried out every 10 °C in the temperature range between 740 °C and 1250 °C with the search for transition temperatures [27]. Figure 1 shows the fraction of AlN, VC, VN, and total VCN versus the temperature. In the model used (FactSage), the VCN fraction is the sum of VC and VN.

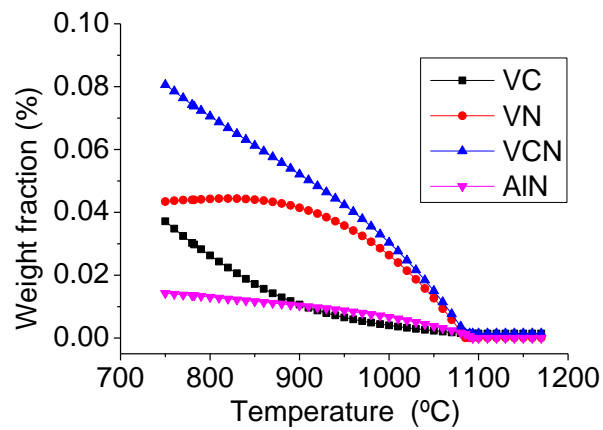


Figure 1. Equilibrium compounds predicted by FactSage.

The values calculated according to the above equations are shown in Figures 2–4. The incubation time (τ) is shown as a function of the temperature (Figure 2). As the effective energy was taken into account in Equation (3) instead of only the energy for bulk diffusion, the values of τ were lower. The critical radius (R_c) for nucleation was calculated from Equation (7) as a function of the temperature (Figure 3).

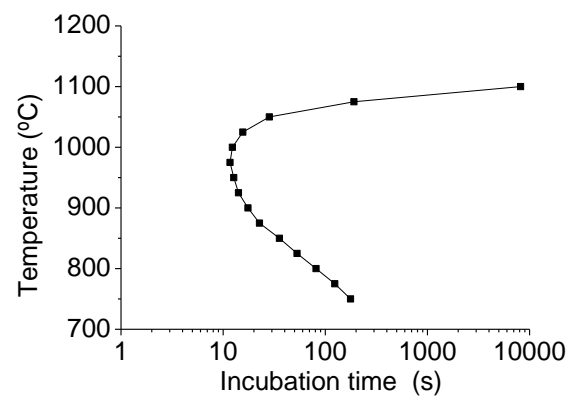


Figure 2. Incubation time vs. temperature (curve P_s) for VCN precipitates.

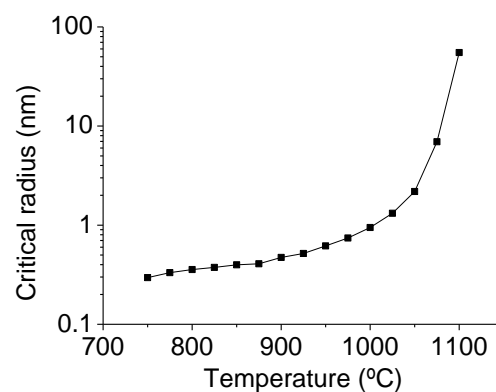


Figure 3. Critical radius size vs. temperature for VCN precipitates.

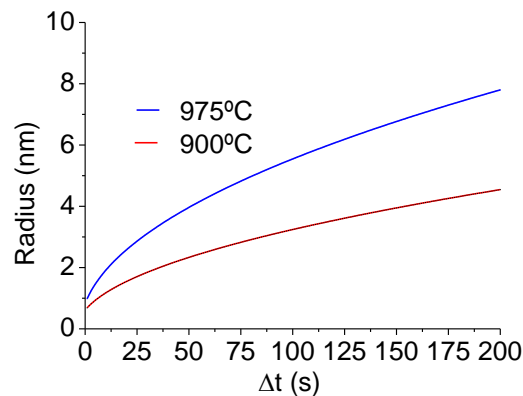


Figure 4. Precipitate size (radius) growth vs. time ($\Delta t > \tau$) for VCN precipitates. Equation (8).

Equation (8) has been applied to the precipitate growth, selecting temperatures of 975 °C (curve nose in Figure 2) and 900 °C. The Δt time starts to be counted after the nucleation period, which was 12 s at 975 °C and 17 s at 900 °C. The value of R_0 was 0.8 nm and 0.5 nm, both multiplied by 1.05, at 975 °C and 900 °C, respectively. The growth of nuclei is shown in Figure 4. The calculations have been performed using parameters extracted from literature [9,10,15,28,29] and shown in Table 2.

Table 2. Parameters used for calculations.

Parameter	Symbol	Value	Reference
Burgers vector	b (m)	2.59×10^{-10}	[9]
Shear modulus	μ (MPa)	4.5×10^4	[9]
Interfacial energy	γ (J·m ⁻²)	0.5	[10,15]
Lattice parameter (VCN)	a (nm)	0.4118	[26]
Bulk diffusion of V	D_V (m ² ·s ⁻¹)	$0.28 \times 10^{-4} e^{(-264,000/RT)}$	[27]
Pipe diffusion	D_P (m ² ·s ⁻¹)	$0.25 \times 10^{-4} e^{(-210,000/RT)}$	[26]
Molar volume of VCN	V_P (m ³ ·mol ⁻¹)	10.65×10^{-6}	[15]
Molar volume of austenite	V_{Fe} (m ³ ·mol ⁻¹)	7.11×10^{-6}	[15]
Dislocation core radius	R_{core} (m)	5.00×10^{-10}	[10]

The term ΔG_V Equation (2) is important in the calculations carried out, whose values at 975 °C and 900 °C were -1.347×10^9 J·m⁻³ and -2.115×10^9 J·m⁻³, respectively.

Dutta et al. [9] checked that the number of particles per unit volume decreased dramatically and this is not predicted by a simple growth model. Such a reduction in the density of particles per unit volume requires particle coarsening. The coarsening of precipitates by coalescence occurs once precipitation is complete, i.e., when the plateau has ended and recrystallization progresses again. Coalescence can be explained by the modified Lifshitz–Slyozov–Wagner theory (MLSW) [29,30], which predicts that while the basic $t^{1/3}$ kinetics of the LSW theory is maintained, the coarsening rate increases as the volume fraction increases, even at very small precipitated volume fraction values.

Coarsening is given by the expression:

$$R^3 = R_0^3 + \frac{8D_V\gamma V_P^2 X_V^i}{9R_g T} \Delta t \quad (9)$$

where R_g is the gas constant and the other parameters have already been explained.

Coarsening is the process by which the smallest precipitates dissolve to the profit of the larger ones, leading to a distribution peak shift to larger sizes. This phenomenon is particularly important when the system reaches the equilibrium precipitate fraction. It is to be noted that coarsening can occur at every stage of the precipitation process [15].

The most striking aspect of Equation (9) is that the mean radius cubed varies with time, as opposed to the squared radius in growth calculations. Coarsening is thus a much slower process than precipitate growth, as is reasonable given that the growth of one particle only occurs by cannibalistic particle growth [22].

Following Equation (9), nucleus growth was calculated for the temperatures of 975 °C and 900 °C. Once again, D_V has been replaced by D_{eff} , which is one order of magnitude higher. The result is shown in Figure 5, where it can be seen that coarsening does not take place at these temperatures and is therefore nil, unlike that shown in Figure 4. This is because the value of D_{eff} , or D_V , is very low at the mentioned temperatures and rises as the temperature increases. In other words, at higher temperatures coarsening by coalescence would also probably take place during precipitation and after this has ended.

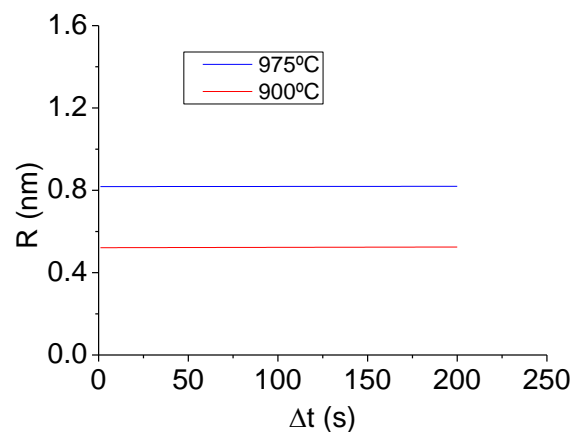


Figure 5. Precipitate size (radius) coarsening vs. time ($\Delta t > \tau$). Equation (9).

3.2. Evolution of Experimental Precipitate Size

The applied strain was 0.35, which was insufficient to promote dynamic recrystallization [31]. At high temperatures (above T_{nr}), the dislocation structure development governs the rates of recovery and recrystallization, which affect the austenite grain size, high temperature strength, and start of precipitation [32].

The resolution of precipitates using the carbon extraction replica technique by TEM is shown in Figure 6a–c, obtained on a specimen strained and quenched in the conditions indicated at the foot of the figure. The spectrum in Figure 6b shows the presence of V on the precipitate indicated by the red arrow in Figure 6a, and the lattice parameter determined from Figure 8c reveals a fcc cubic lattice with a value of $a = 0.413$ nm, which is identified, in accordance with the reference value found in the literature [22], as a vanadium carbonitride (VCN). The two unassigned peaks are Fe and Ni (6.4 keV and 7.4 keV, respectively). They may be due to grid impurities or residues from preparation in the evaporator. It is well known that the copper peak always appears in the carbon extraction replica technique and is due to the copper support grid.

On the other hand, the particle size distribution and determination of the average particle have been obtained by measuring an average number of 200 particles on the tested specimens. Figure 7 shows a log-normal distribution that corresponds to a holding time of 50 s at 900 °C, and a bimodal distribution corresponding to holding times of 250 s and 800 s, respectively, with a weighted mean size (diameter \bar{D}) of 11.2 nm, 19.2 nm, and 20.4 nm, respectively. Other authors have found similar sizes of V(C,N) precipitates [33].

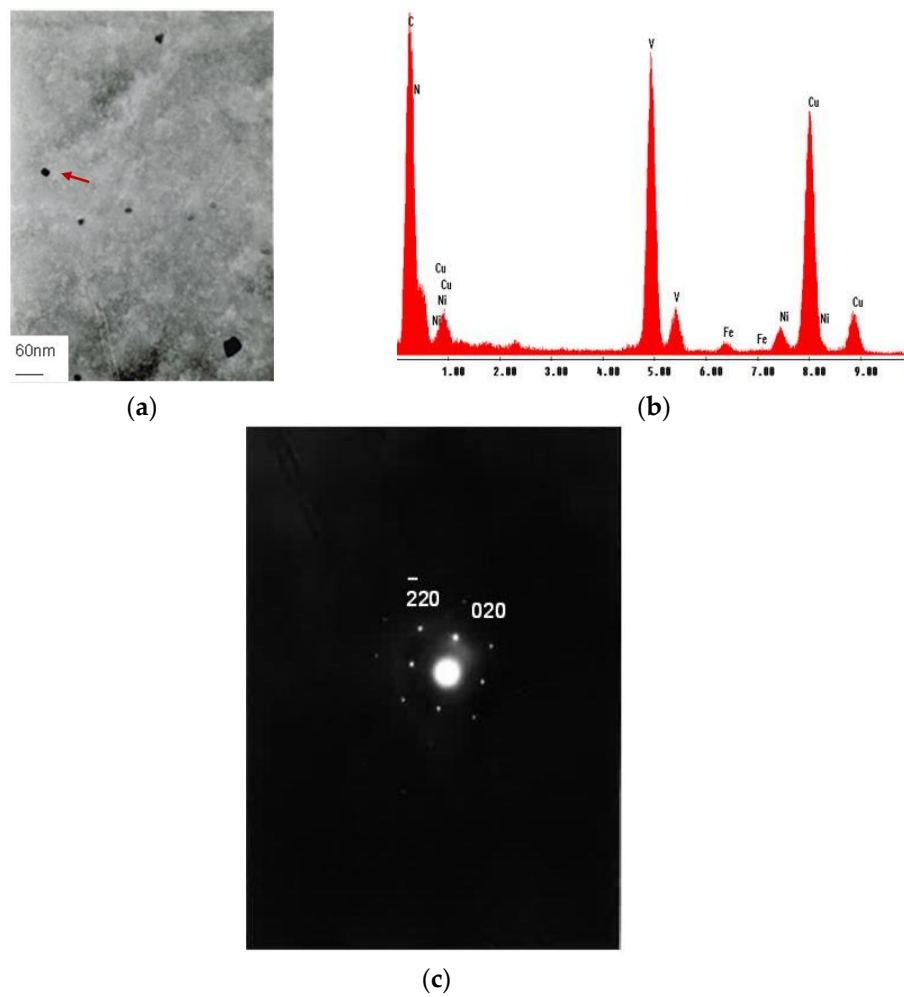


Figure 6. TEM images of steel used. (a) Image showing precipitates for specimen tested at reheating temperature of 1200 °C/10 min; Def. temp.= 900 °C; strain = 0.35; strain rate = 3.63 s⁻¹; holding time = 250 s; (b) EDAX spectrum of precipitate; (c) Electron diffraction image.

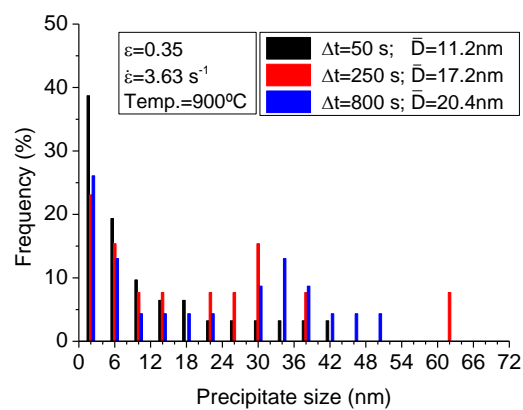


Figure 7. Size distribution of precipitates for specimen tested at reheating temperature of 1200 °C for 10 min, deformation temperature of 900 °C, and holding times of 50 s, 250 s, and 800 s.

If we accept that the precipitates grow once they are nucleated, then moment zero of growth coincides with the nucleation time (τ) and Δt will be the sample holding time after τ . Figure 8 shows a representation of the average precipitate growth at a temperature of 900 °C, where the size is given by

the mean radius ($R = \bar{D}/2$). The holding times after the nucleation time were 50 s, 250 s, and 800 s, minus the value of 17 s corresponding to the calculated incubation time at 900 °C. At first sight there are seen to be two growth laws. Between the first two points, the nucleus grows notably; between the last two, it barely grows. These two laws obey Equations (8) and (9), respectively, and show that the precipitates grow during precipitation but that coarsening by coalescence does not take place. As coalescence does not occur, it has already been seen that Equation (9) is a constant at 900 °C (Figure 5). If a horizontal line is drawn from the final point, with coordinates at 783 s; 10.2 nm, to its intersection with the quadratic curve, the intersection point is determined to be at coordinates 275 s; 10.2 nm, which means that precipitation has ended 275 s after the nucleation time (17 s).

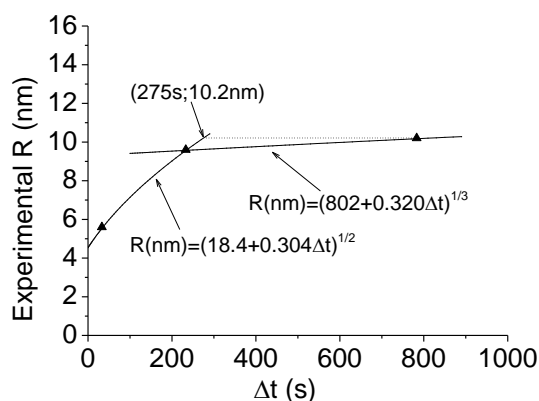


Figure 8. Experimental growth and coarsening of precipitates.

From Figure 8, in particular from the quadratic equation, it is possible to deduce the nucleus radius (R_0). This indicates a size of 4.3 nm when $\Delta t = 0$, corresponding to the nucleus size at 900 °C, which is greater than the nucleus radius calculated at the theoretical curve nose, which was approximately 0.5 nm. It is necessary to highlight the conceptual difference between the theoretical and experimental incubation time curves, respectively. The calculated and experimental nucleation times do not have the same meaning. The nucleation time calculated at any temperature means the time necessary for the formation of a number N of nuclei, of size R_0 , whose growth continues when the precipitate radius reaches a size of $1.05R_0$. The experimental nucleation time refers to the time necessary for the pinning forces to exceed the driving forces for recrystallization, temporarily inhibiting the progress of recrystallization [34]. On the other hand, the carbon extraction replica technique does not easily detect precipitates with sizes of less than 1 nm.

The results confirm that the time of 275 s deduced for the end of precipitation, to which the 17 s of the nucleation time must be added, coincides approximately with the experimentally determined precipitation end time [35].

In other words, to explain the increase in the average precipitate size, it is sufficient to use the growth equation, and coalescence can be ignored. On the other hand, from the holding time of 50 s to the holding time of 250 s, the measured precipitate radius has increased from 5.6 nm to 9.6 nm, an increase of 4 nm. If the times of 50 s and 200 s are inserted in Figure 4, subtracting from both the calculated incubation time (17 s) at 900 °C, it is seen that the nucleus radius increases from 2 nm to 4.6 nm. Therefore, the calculated and experimental growth rates are similar.

It is thus deduced from both the experimental and theoretical points of view that precipitate growth between the start (P_s) and end of precipitation (P_f) can be predicted by the growth equation, as coarsening is not taking place, so it is not necessary to include the coalescence equation. The main difference between the calculated and experimental values is the nucleus size.

4. Conclusions

In conclusion, the calculated mean nucleus radius was approximately 0.5 nm and the experimental average radius was 4.3 nm at the temperature of 900 °C. This is due to the conceptual difference between the theoretical and experimental incubation time curves, respectively. The precipitate size growth rate between the experimentally determined P_s and P_f practically coincides with the calculated growth rate. Both are expressed by a quadratic growth equation in such a way that the coalescence of precipitates during precipitation is not taking place and can be ruled out. Since the effective diffusion coefficient (D_{eff}) parameter increases notably with the temperature, coarsening can take place at very high temperatures.

Acknowledgments: We acknowledge the financial support of the Spanish CICYT (Project MAT 2011-29039-C02-02).

Author Contributions: Sebastián F. Medina conceived and designed the work and also performed and interpreted the results; Inigo Ruiz-Bustanza and José Robla made calculations and drew graphs; Jessica Calvo did thermodynamic calculations and drew the corresponding graphs. All contributed to the writing of the paper, especially S.F. Medina.

Conflicts of Interest: The authors declare no conflict of interest.

References

1. Gómez, M.; Medina, S.F.; Quispe, A.; Valles, P. Static recrystallization and induced precipitation in a low Nb microalloyed steel. *ISIJ Int.* **2002**, *42*, 423–431. [[CrossRef](#)]
2. Medina, S.F.; Quispe, A.; Gómez, M. Strain induced precipitation effect on austenite static recrystallization in microalloyed steels. *Mater. Sci. Technol.* **2003**, *19*, 99–108. [[CrossRef](#)]
3. Andrade, H.L.; Akben, M.G.; Jonas, J.J. Effect of molybdenum, niobium, and vanadium on static recovery and recrystallization and on solute strengthening in microalloyed steels. *Metall. Trans. A* **1983**, *14*, 1967–1977. [[CrossRef](#)]
4. Kwon, O. A technology for the prediction and control of microstructural changes and mechanical properties in steel. *ISIJ Int.* **1992**, *32*, 350–358. [[CrossRef](#)]
5. Luton, M.J.; Dorvel, R.; Petkovic, R.A. Interaction between deformation, recrystallization and precipitation in niobium steels. *Metall. Trans. A* **1980**, *11*, 411–420. [[CrossRef](#)]
6. Gómez, M.; Rancel, L.; Medina, S.F. Effects of aluminium and nitrogen on static recrystallization in V-microalloyed steels. *Mater. Sci. Eng. A* **2009**, *506*, 165–173. [[CrossRef](#)]
7. Gómez, M.; Medina, S.F. Role of microalloying elements on the microstructure of hot rolled steels. *Int. J. Mater. Res.* **2011**, *102*, 1197–1207. [[CrossRef](#)]
8. Kwon, O.; DeArdo, A. Interactions between recrystallization and precipitation in hot-deformed microalloyed steels. *Acta Metall. Mater.* **1990**, *39*, 529–538. [[CrossRef](#)]
9. Dutta, B.; Valdes, E.; Sellars, C.M. Mechanisms and kinetics of strain induced precipitation of Nb(C,N) in austenite. *Acta Metall. Mater.* **1992**, *40*, 653–662. [[CrossRef](#)]
10. Dutta, B.; Palmiere, E.J.; Sellars, C.M. Modelling the kinetics of strain induced precipitation in Nb microalloyed steels. *Acta Mater.* **2001**, *49*, 785–794. [[CrossRef](#)]
11. Russel, K.C. Nucleation in solids: The induction and steady state effects. *Adv. Colloid. Interface Sci.* **1980**, *13*, 205–318. [[CrossRef](#)]
12. Kampmann, R.; Wagner, R. *A Comprehensive Treatment, Materials Science and Technology*; Cahn, R.W., Ed.; VCH: Weinheim, Germany, 1991; pp. 213–303.
13. Wiskel, J.B.; Lu, J.; Omotoso, O.; Ivey, D.G.; Henein, H. Characterization of precipitates in a microalloyed steel using quantitative X-ray diffraction. *Metals* **2016**, *6*, 90. [[CrossRef](#)]
14. Fujita, N.; Bhadeshia, H.K.D.H. Modelling precipitation of niobium carbide in austenite: Multicomponent diffusion, capillarity and coarsening. *Mater. Sci. Technol.* **2001**, *17*, 403–408. [[CrossRef](#)]
15. Maugis, P.; Gouné, M. Kinetics of vanadium carbonitride precipitation in steel: A computer model. *Acta Mater.* **2005**, *53*, 3359–3367. [[CrossRef](#)]
16. Sun, W.P.; Militzer, M.; Bai, D.Q.; Jonas, J.J. Measurement and modelling of the effects of precipitation on recrystallization under multipass deformation conditions. *Acta Metall. Mater.* **1993**, *41*, 3595–3604. [[CrossRef](#)]

17. Salas-Reyes, A.E.; Mejía, I.; Bedolla-Jacuinde, A.; Boulaajaj, A.; Calvo, J.; Cabrera, J.M. Hot ductility behavior of high-Mn austenitic Fe-22Mn-1.5Al-1.5Si-0.45C TWIP steels microalloyed with Ti and V. *Mater. Sci. Eng. A* **2014**, *611*, 77–89. [[CrossRef](#)]
18. Mejía, I.; Salas-Reyes, A.E.; Bedolla-Jacuinde, A.; Calvo, J.; Cabrera, J.M. Effect of Nb and Mo on the hot ductility behavior of a high-manganese austenitic Fe-21Mn-1.3Al-1.5Si-0.5C TWIP steel. *Mater. Sci. Eng. A* **2014**, *616*, 229–239. [[CrossRef](#)]
19. Zurob, H.S.; Hutchinson, C.R.; Brechet, Y.; Purdy, G. Modeling recrystallization of microalloyed austenite: Effect of coupling recovery, precipitation and recrystallization. *Acta Mater.* **2002**, *50*, 3075–3092. [[CrossRef](#)]
20. Perrard, F.; Deschamps, A.; Maugis, P. Modelling the precipitation of NbC on dislocations in α -Fe. *Acta Mater.* **2007**, *55*, 1255–1266. [[CrossRef](#)]
21. Medina, S.F.; Hernández, C.A.; Ruiz, J. Modelling austenite flow curves in low alloy and microalloyed steels. *Acta Mater.* **1996**, *44*, 155–163.
22. Gladman, T. *The Physical Metallurgy of Microalloyed Steels*; The Institute of Materials: London, UK, 1997; pp. 28–56.
23. Perez, M.; Courtois, E.; Acevedo, D.; Epicier, T.; Maugis, P. Precipitation of niobium carbonitrides in ferrite: Chemical composition measurements and thermodynamic modelling. *Phil. Mag. Lett.* **2007**, *87*, 645–656. [[CrossRef](#)]
24. Radis, R.; Schlacher, C.; Kozeschnik, E.; Mayr, P.; Enzinger, N.; Schröttner, H.; Sommitsch, C. Loss of ductility caused by AlN precipitation in Hadfield steel. *Metall. Mater. Trans. A* **2012**, *43*, 1132–1139. [[CrossRef](#)]
25. Perez, M.; Deschamps, A. Microscopic modelling of simultaneous two phase precipitation: Application to carbide precipitation in low carbon steels. *Mater. Sci. Eng. A* **2003**, *360*, 214–219. [[CrossRef](#)]
26. FSstel Database. Available online: <http://www.factsage.com> (accessed on 4 December 2010).
27. Bale, C.W.; Bélisle, E.; Chartrand, P.; Degterov, S.A.; Eriksson, G.; Hack, K.; Jung, I.H.; Kang, Y.B.; Melancon, J.; Pelton, A.D.; et al. FactSag thermo-chemical software and databases—Recent developments. *Calphad* **2009**, *33*, 295–311. [[CrossRef](#)]
28. Mukherjee, M.; Prahla, U.; Bleck, W. Modelling the strain-induced precipitation kinetics of vanadium carbonitride during hot working of precipitation-hardened ferritic-pearlitic steels. *Acta Mater.* **2014**, *71*, 234–254. [[CrossRef](#)]
29. Oikawa, H. Lattice diffusion in iron—a review. *Tetsu Hagane* **1982**, *68*, 1489–1497.
30. Ardell, J. The effect of volume fraction on particle coarsening: Theoretical considerations. *Acta Metall.* **1972**, *20*, 61–71. [[CrossRef](#)]
31. Badjena, S.K. Dynamic recrystallization behavior of vanadium micro-alloyed forging medium carbon steel. *ISIJ Int.* **2014**, *54*, 650–656. [[CrossRef](#)]
32. Kostryzhev, A.G.; Mannan, P.; Marenych, O.O. High temperature dislocation structure and NbC precipitation in three Ni-Fe-Nb-C model alloys. *J. Mater. Sci.* **2015**, *50*, 7115–7125. [[CrossRef](#)]
33. Nafisi, S.; Amirkhiz, B.S.; Fazeli, F.; Arafin, M.; Glodowski, R.; Collins, L. Effect of vanadium addition on the strength of API X100 linepipe steel. *ISIJ Int.* **2016**, *56*, 154–160. [[CrossRef](#)]
34. Gómez, M.; Medina, S.F.; Valles, P. Determination of driving and pinning forces for static recrystallization during hot rolling of a Nb-microalloyed steel. *ISIJ Int.* **2005**, *45*, 1711–1720. [[CrossRef](#)]
35. Medina, S.F.; Quispe, A.; Gomez, M. New model for strain induced precipitation kinetics in microalloyed steels. *Metall. Mater. Trans. A* **2014**, *45*, 1524–1539. [[CrossRef](#)]

